Eddy Subduction in a Model of the Subtropical Gyre

W. HAZELEGER AND S. S. DRIJFHOUT

Royal Netherlands Meteorological Institute, de Bilt, the Netherlands

(Manuscript received 28 October 1998, in final form 26 April 1999)

ABSTRACT

Subduction is the process by which fluid transfers from the mixed layer to the interior of the ocean. South of the Gulf Stream extension, 18° mode water is formed in a region of high subduction rates. In this region there is high mesoscale eddy activity. In the present study the role of eddies in modifying the large-scale subduction into mode water is investigated. An eddy-resolving isopycnic ocean model with mixed layer physics included and coupled to an atmospheric anomaly model is used for this purpose. The geometry and forcing of the model are idealized.

Annual mean subduction rates into mode water up to 200 m yr^{-1} are found south of the Gulf Stream extension. The eddy contribution to the annual subduction is estimated by comparing the annual mean subduction rates, obtained from monthly mean quantities, with the total subduction rates (i.e., eddy plus mean contributions). The latter are determined by integrating the detrainment rates over the period when fluid is irreversibly detrained. Eddy subduction rates up to 100 m yr^{-1} are found. The high-frequency variability enhances the annual mean subduction by almost a factor 2.

The subduction is compared to annual net detrainment. The latter is related to the so-called shallow Ekman overturning. The eddy contribution to this overturning is determined by calculating divergence of the eddy transports in mode water as well as comparing results from the eddy-resolving version of the model with results from a coarse resolution version of the model. The results show an eddy-induced enhancement of the Ekman overturning. Conclusions are drawn with regard to parameterization of eddy subduction and eddy-induced changes of the Ekman overturning.

1. Introduction

The importance of water mass formation and subduction in the coupled ocean–atmosphere climate system has recently reemerged from both observational (Sutton and Allen 1997; Zhang and Levitus 1997) and modeling (Zorita and Frankignoul 1997) studies. The decadal timescale of the dominant modes of low-frequency atmospheric variability in the midlatitudes (e.g., the North Atlantic Oscillation) may be determined by the propagation of subsurface thermal anomalies through the subtropical gyre. Such thermal anomalies can be formed in the mixed layer by the varying atmospheric forcing and subsequently be subducted to the subsurface layers. The most distinct water mass formed in the subtropical gyre is 18°C mode water (Worthington 1959). This voluminous water mass forms south of the Gulf Stream extension. Mode water formation is the result of wintertime cooling followed by springtime warming of the mixed layer. The associated deepening of the mixed layer in the winter and shallowing in the spring causes large volumes of water to subduct (Woods 1985). In this paper we investigate the mass exchange between the mixed layer and the interior in the subtropical gyre with specific attention to the formation of mode water.

As we consider the role of *entrainment*, *detrainment*, and *subduction* and their relations in formation of subtropical mode water, it is appropriate to define these terms precisely. We define *entrainment* as the mass transfer from the interior to the mixed layer due to deepening of the mixed layer by turbulent mixing. *Detrainment* is defined as the mass transfer from the mixed layer to the interior due to shallowing (restratification) of the mixed layer by heating, freshening and/or decreasing wind input. In the present paper, we will diagnose entrainment and detrainment in an Eulerian framework. Note that horizontal advection in the presence of a horizontal gradient in mixed layer depth may also lead to deepening/shallowing of the mixed-layer depth without the action of turbulent mixing or restratification. Only entrainment/detrainment is associated with a mass exchange between the mixed layer and the thermocline. *Subduction* is that part of the detrained fluid that is not reentrained (elsewhere) in the mixed layer within the same seasonal cycle. This definition

Corresponding author address: Dr. W. Hazeleger, Royal Netherlands Meteorological Institute (KNMI), P.O. Box 201, 3730 AE, de Bilt, the Netherlands.
E-mail: hazelege@knmi.nl

applies in a Lagrangian framework. However, the subduction will be estimated from the Eulerian fields. Detrainment and entrainment can be regarded as instantaneous quantities, while subduction is always defined as an integrated quantity over one or several seasonal cycles. Sometimes the term *obduction* is used for the opposite of subduction.

There have been two approaches toward a theoretical description of the formation of water masses. The first approach is based on the heat budget of a volume of water between two isopycnals (Walin 1982). According to Walin's algorithm, water mass transformation rates can be determined from the surface heat fluxes. This method has been clarified and extended by Tziperman (1986), Garrett et al. (1995), and Garrett and Tandon (1997). The second approach focuses on the kinematics of the ocean circulation (e.g., Cushman-Roisin 1987). The transfer of water from the mixed layer into the interior of the ocean is determined with the vertical and the horizontal velocity at the shoaling mixed layer base. Both methods can be used as a diagnostic tool to quantify water mass formation from oceanographic data (e.g., Speer and Tziperman 1992; Marshall et al. 1993; Qiu and Huang 1995). The heat-flux-based method does not distinguish the mixed layer from the interior, in contrast to the kinematical method. Therefore, the kinematical method is more appropriate for this study.

In the present study we focus on subduction in an eddying ocean, that is, the contribution of both the mean flow and the eddies to subduction. The large-scale subduction rate associated with the mean flow is $O(100\ \text{m yr}^{-1})$ (see Marshall et al. 1993). In the region where mode water is formed the ocean is populated with mesoscale eddies and the large-scale subduction rate associated with the mean flow may not be representative. Follows and Marshall (1994) found an eddy-induced subduction rate of approximately $150\ \text{m yr}^{-1}$ using scaling arguments. Comparable values have been found by Spall (1995) in a high-resolution isopycnic channel model of an idealized jet. These estimates are based on highly idealized configurations within rather limited domains. Whether such values are relevant to the subduction on the gyre scale is not clear. Recent observations and modeling results of the biogeochemical cycle in the North Atlantic subtropical gyre suggest a large contribution of the eddies (Oschlies and Garcon 1998; McGillicudy et al. 1998).

Observational data are generally too sparse to deduce the contribution of eddies to subduction. A long-term synoptic high-resolution dataset is needed to clarify the role of eddies on the gyre scale. Because such a dataset is not available, a numerical model is used to study the role of eddies in subduction. Here an isopycnic ocean model with an embedded mixed layer model is used. The model is coupled to an atmospheric anomaly model. The coupled isopycnic–mixed layer model is ideal for water mass studies. The model configuration is idealized, but the processes and the tools we work out here are expressed most clearly in the present configuration. The aim of this study is to quantify the contribution of eddies to subduction on the gyre scale in the numerical model.

The numerical model and the forcing are introduced in section 2. Section 3 describes some general features of the model solution. The kinematical method is used to estimate the annual subduction into mode water by the mean flow (section 4a). Furthermore, the contribution of the eddies to annual subduction into mode water is estimated (see section 4b). Marshall (1997) extended the kinematical method to include eddies. He considered subduction at meandering outcrops in a two-dimensional model without a seasonal cycle. According to Marshall, the correlation between the local detrainment rate and the area over which a subsurface isopycnic layer outcrops results in an eddy contribution to the time-mean subduction. When a seasonal cycle is included and a three-dimensional circulation is considered, the concept of Marshall is not applicable straightforwardly. Therefore, a more direct approach is used in this study. The eddy contribution to subduction is estimated by comparing the subduction by the mean flow with the total subduction, that is, the mean plus eddy contribution.

In section 5 we focus on the annual mean of the entrainment and detrainment rates and compare these with the pattern of annual subduction. Regions of annual-mean entrainment and annual-mean detrainment are associated with a vertical mean overturning. The eddy contribution to this overturning is also determined in section 5.

In section 6 the results are discussed. A pathway of ventilated water is presented, and we discuss the difference between flow in the two-dimensional and three-dimensional context. The implications for heat transport and parameterization of eddy transports in coarse-resolution models are discussed and related to the parameterization proposed by Marshall (1997) in a two-dimensional model. Finally, in section 7 a summary is given and conclusions are drawn.

2. The numerical model and forcing

In this study results from two experiments are discussed. The two experiments are performed in the same model context, but have been run with a different horizontal resolution and a different diffusion and friction parameterization. In this section the numerical ocean model and the forcing are described. We will denote the experiment with the fine-resolution version of the model as experiment 1 and with the coarse-resolution version of the model as experiment 2.

a. Ocean model

The ocean model is an isopycnic primitive equation model with mixed layer physics included. The model

allows us to focus on separate model layers that represent distinct water masses. The original ocean model was presented by Bleck and Boudra (1986). Various versions of the present model have been used by Drijfhout (1994a, b), Hazeleger and Drijhout (1998, hereafter HD98), and Hazeleger and Drijfhout (1999). We refer to these papers for more details on the model.

The model has seven isopycnic layers. The density difference between the layers is 0.8 kg m^{-3} (equivalent to a temperature difference of 4°C when salinity is kept constant). The deepest layer has a density corresponding to 1026.6 kg m^{-3} (i.e., an average temperature of 2° at the average salinity of 35 psu). In the isopycnic layers salinity is advected and diffused. The temperature is calculated as a residual according to the (linear) equation of state that we use (see Bleck et al. 1992). In the remainder we will denote the isopycnic layers by their equivalent temperature, which is the average temperature the layer would have if the average salinity would be 35 psu.

In experiment 1 the model has a resolution of 37 km. A biharmonic friction and diffusion is used to parameterize subgrid processes (Bleck and Boudra 1986). The biharmonic friction parameter is 1×10^{11} m^4 s^{-1}. The same value is chosen for the biharmonic diffusivity. Under the present forcing a vigorous eddy field can be simulated with this resolution and parameterization (see section 2b). With a grid size smaller than 37 km the level of eddy kinetic energy and potential energy increases, but no qualitative changes occur with respect to the mesoscale eddies (Drijfhout 1994a). In experiment 2 the horizontal resolution is 74 km. A harmonic Laplacian friction and diffusion parameterization is used instead of the biharmonic friction and diffusion. The viscosity parameter is 3000 m^2 s^{-1}, the diffusivity parameter is 1500 m^2 s^{-1}. Eddies are not resolved with this resolution and amount of friction and diffusion.

In both model versions diapycnal diffusion is incorporated with a diffusion coefficient of 10^{-4} m^2 s^{-1}. The domain of the model is closed and describes an idealized North Atlantic midlatitude jet and the subtropical gyre. A stepwise continental shelf break with a width of 500 km is incorporated at the western boundary of the basin (see Drijfhout 1994a).

The isopycnic ocean model is coupled to a bulk mixed layer model. The mixed layer model is a Kraus–Turner mixed layer model based on the algorithm presented by Bleck et al. (1989). This model is suitable because the vertical homogeneous structure of the isopycnal layers is retained in the mixed layer. Although more sophisticated mixed layer parameterizations are available, the bulk mixed layer model performs well considering the present idealized context (see HD98 for a discussion). Entrainment of subsurface water or detrainment of mixed layer water takes place according to the turbulent kinetic energy (TKE) generation by the surface fluxes. When the net generation of TKE is positive, the mixed layer deepens. This process implies an increase of potential energy of the water column. The new mixed layer depth is determined by a balance between the generation of TKE and the increase of potential energy. When the net generation of TKE is negative the mixed layer shoals to the depth where the positive input of TKE by the wind stress equals the negative input by the buoyancy fluxes, that is, the Monin Obukhov length. For more specific details on the algorithm we refer to Bleck et al. (1989).

b. Forcing

Experiment 1 was spun up from the equilibrium state of the coarse-resolution version of the model discussed by Hazeleger and Drijfhout (1999). We slightly changed the forcing profiles to reduce the overshoot of the Gulf Stream in the model.

The present forcing is shown in Fig. 1. The zonally averaged freshwater flux is prescribed. The negative freshwater flux is high in the north. In the subtropical gyre the evaporation is less strong. This is necessary to ensure a vanishing basin-integrated freshwater flux. With this forcing, a circulation and water mass distribution is simulated that is typical for the subtropical North Atlantic (see section 3).

As the basin width at the latitude of the maximum anticyclonic wind stress curl is about one-third of the width of the subtropical Atlantic, the amplitude of the wind stress has been enhanced by a factor of 3 compared to observations. In this way, the linear component of the western boundary current will have the correct magnitude. Due to nonlinearities and rectification of the flow by its instabilities, the flow becomes much more unstable than with a three times weaker wind in a three times larger basin. The Rossby radius of deformation (40–50 km) is only marginally larger than the grid spacing (37 km). However, the enhanced winds, together with the weak diffusion and the free slip lateral boundary conditions, lead to a vigorous eddy field in which the enstrophy cascade is well represented. The advective timescale of the subtropical gyre, however, becomes much too short after the wind enhancement (i.e., 1–2 yr). To obtain a realistic ratio between advection and forcing timescales, the seasonal cycle is shortened by a factor of 3.

The Ekman pumping and the entrainment/detrainment rates are increased due to the wind enhancement. But due to the shortened seasonal cycle the net annual detrainment and the annual subduction rates (see section 4) become realistic. The overall flow field and thickness distribution are insensitive to the changes. When referring to years in this study, we mean one seasonal cycle (120 days).

In the final stage of the spinup at high resolution, the temperature was restored to the zonally averaged and seasonally dependent apparent temperature shown in Fig. 1. After 80 years a cyclostationary state was reached and the heat fluxes were diagnosed from the

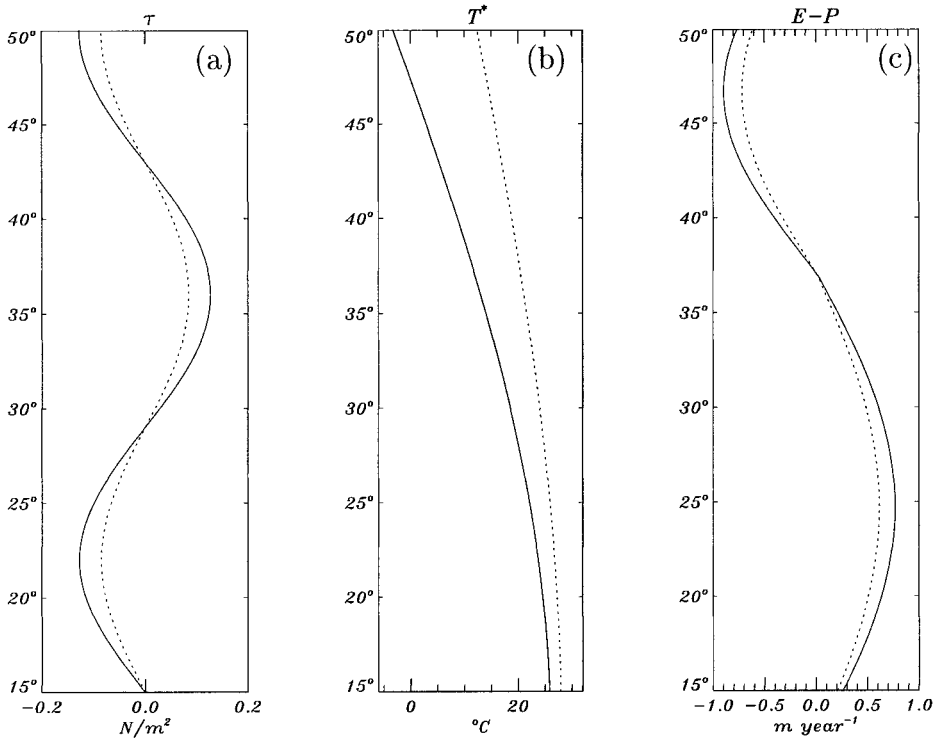

FIG. 1. Zonally averaged forcing profiles (continuous line = winter, dotted line = summer). (a) Wind stresss, (b) apparent temperature, and (c) evaporation minus precipitation.

restoring boundary condition for temperature. Then the model was forced by an interpolated climatological heat flux $\overline{Q}$ plus an anomalous heat flux Q'_H. The climatological heat flux was calculated as an average of the monthly mean values of the last 20 years of the spinup. So anomalous fields are defined with respect to the seasonal cycle that is contained in the mean fields. The actual mean fields are always an interpolated value between two monthly mean fields.

The anomalous heat flux is determined with a drag relation. It depends on the difference between the anomalous SST and anomalous air temperature:

$$Q = \overline{Q} + Q'_H = \overline{Q} + \rho c_p C_H \epsilon |\mathbf{u}_a|(T'_a - T'_{oc}), \quad (1)$$

where $C_H = 1.3 \times 10^{-3}$ is the drag coefficient and T'_{oc} is the difference between the simulated SST and the SST diagnosed after the spinup. The anomalous air temperature T'_a in the atmospheric boundary layer is determined with a prognostic equation, which includes advection, diffusion, and forcing ($-Q'_H$) of T'_a (see Luksch and von Storch 1992; Drijfhout and Walsteijn 1998; Hazeleger and Drijfhout 1999). The heat flux consists of a sensible and latent heat flux. The ratio between both heat fluxes is called the Bowen ratio. For oceanographic conditions the Bowen ratio is 3 (Stull 1988). Therefore ϵ, which is the ratio of the total heat flux to the sensible heat flux, is chosen to be 4. In principle SST anomalies are damped by the anomalous heat flux.

The coupled model was run for 70 years. The last 19 years have been used in the subsequent analysis as they show negligible drift. During this period, every three days the thickness, velocity, and density fields were saved, both in the mixed layer and in the 18°C layer. The thickness and density fluxes were integrated for each three day interval. The data enable us to calculate the higher-order eddy statistics.

In experiment 2 the same strategy was chosen. The model was initialized with the statistically steady state of the uncoupled version of the fine-resolution model. The model was then run for 120 years with the same forcing as in experiment 1 (Fig. 1). Again the heat fluxes were diagnosed and the coupled model was run for another 60 years. A new equilibrium was reached. The last 19 years have been used for the analysis.

3. Basic features of the model solution

In this section some characteristics of the model solution in experiment 1 and experiment 2 are presented. The results are based on data of the last 19 years of both integrations.

In experiment 1 the model exhibits substantial variability. Internal variability under constant forcing associated with instabilities of the mean flow has been shown by other authors as well (e.g., Cox 1987). During the last 20 years of the model integration, the average mode water thickness and the average kinetic energy

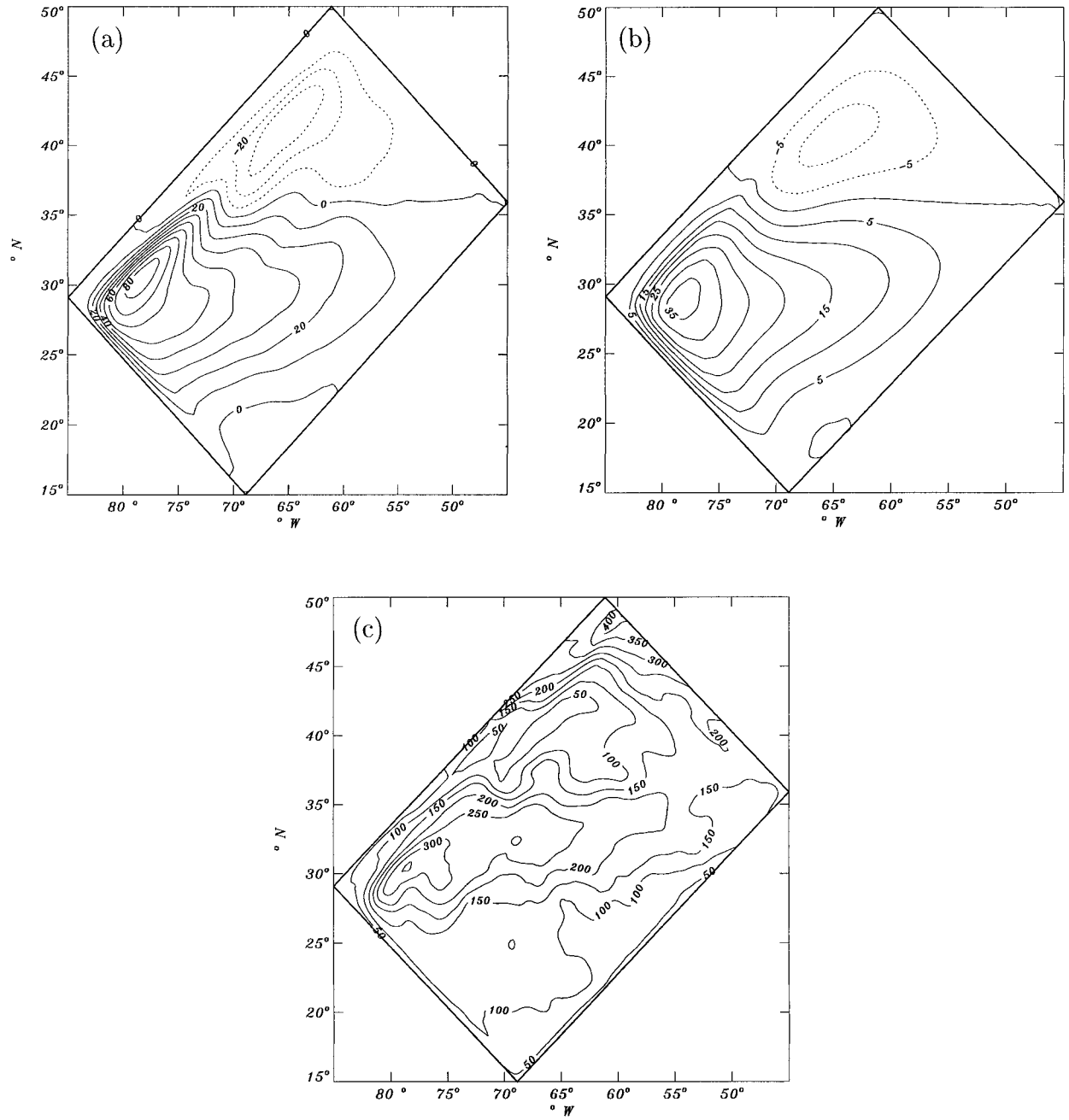

FIG. 2. Time-averaged barotropic streamfunction in Sv (Sv $\equiv 10^6$ m^3 s^{-1}) for (a) expt 1 and (b) expt 2. (c) Averaged mixed layer thickness (m) in Mar for expt 1.

hardly changed. In experiment 2 no internal variability occurred.

Figures 2a,b show the barotropic streamfunction averaged over the 19-yr period for experiments 1 and 2. In experiment 1 the model simulates a strong subtropical gyre consistent with the geometry and the applied forcing. The maximum transport is 80 Sv (Sv $\equiv 10^6$ m^3 s^{-1}), which is somewhat less than the observed transport in the Gulf Stream (Pierce and Joyce 1988). The barotropic streamfunction in experiment 2 is similar, but the transport is much weaker (40 Sv).

The averaged mixed layer depth in March for experiment 1 is shown in Fig. 2c. In March the maximum mixed layer depth is reached. The mixed layer depths are comparable to estimates from observations. Marshall et al. (1993) found maximum mixed layer depths of 300 m in the Gulf Stream extension. It is crucial to capture these deep mixed layers, as in these regions most sub-

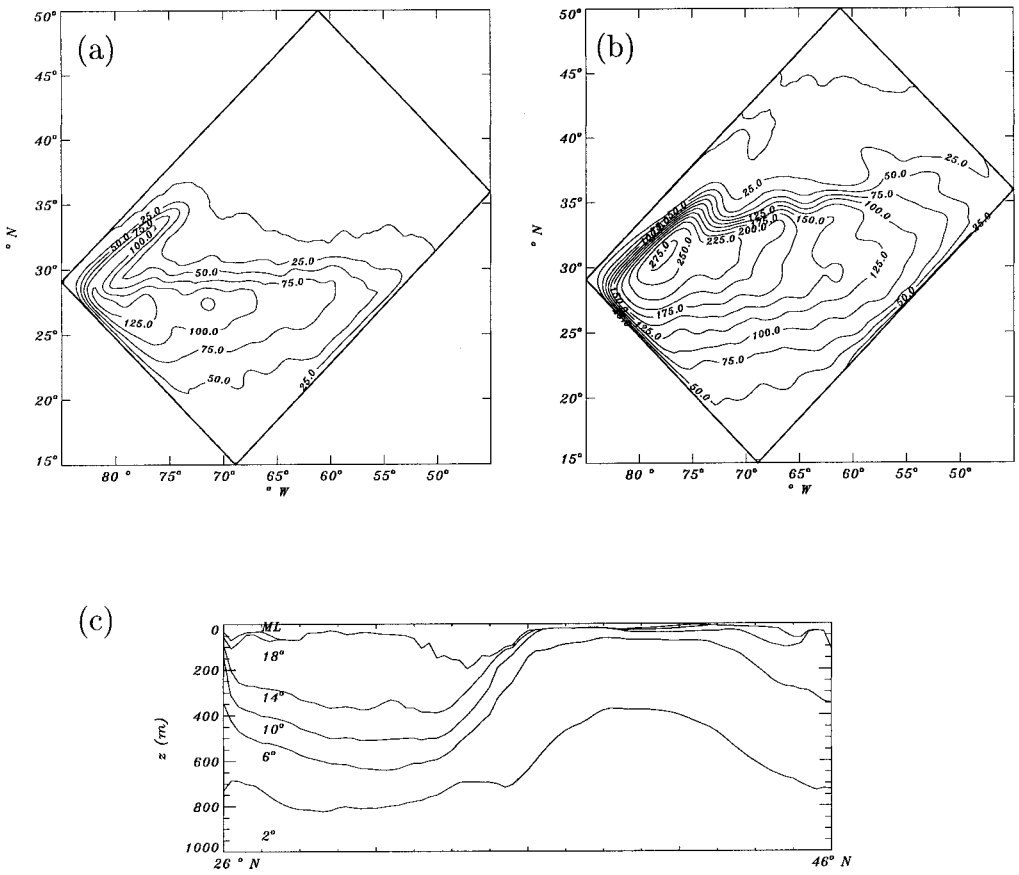

FIG. 3. Time-averaged mode water thickness (m) in (a) Mar and (b) Jul in expt 1. (c) Cross section from the southwest to the northeast of the domain, in Jul in expt 1.

duction takes place. In September the mixed layer is at a minimum of less than 25 m in the subtropical gyre. In the western boundary current region, cooling-driven entrainment causes the mixed layers to be relatively deep throughout the year. In experiment 2 the maximum is more confined to the western boundary current region and the mixed layer is less deep.

The horizontal distribution of the thickness of the 18°C layer is shown in Figs. 3a and 3b for experiment 1. This layer is the thickest subsurface layer above the main thermocline. It is the model equivalent of mode water. The mode water layer is relatively thin in March when the mixed layers are deep. During spring and summer the outcrop moves northward in response to the buoyancy forcing. Also, the mode water becomes thicker due to the shoaling of the mixed layer. The cross section presented in Fig. 3c is taken in July when most detrainment has taken place. It shows that mode water is well represented by the 18°C layer in experiment 1. Also the typical bowl shape of the thermocline in the subtropical gyre is clearly visible. The thick mixed layers around 35°N are associated with the region where entrainment persists throughout the year due to advection of warm water.

Considering the simple geometry of the model and the idealized forcing, the model simulates a circulation and water mass distribution that characteristic for the North Atlantic subtropical gyre.

4. Subduction

a. Subduction by the mean flow

In this section the subduction by the mean flow is estimated using the kinematical method. The contribution of the eddies is estimated in the next section. The seasonal cycle in the surface forcing causes the mixed layer to shoal in spring and deepen during the rest of the year. The deepening of the mixed layer by the turbulent fluxes can be expressed in an entrainment velocity at the base of the mixed layer:

$$w_e = \frac{\partial h_{\mathrm{ml}}}{\partial t} + \mathbf{u}_{\mathrm{mb}} \cdot \nabla h_{\mathrm{ml}} + w_{\mathrm{mb}}. \qquad (2)$$

Here, h_{ml} is the mixed layer depth, $\mathbf{u}_{\mathrm{mb}} = (u_{\mathrm{mb}}, v_{\mathrm{mb}})$ and w_{mb} are the horizontal and vertical velocities at the mixed layer base. So, the entrainment rate is balanced by a local change in mixed layer depth, a lateral advection, and a vertical velocity at the base of the mixed layer. Here w_e is positive when the deepening of the

mixed layer is larger than the divergence of the horizontal transport in the mixed layer, that is, $\partial h_{\rm ml}/\partial t > -\nabla \cdot \mathbf{U}$ [where $\mathbf{U} = \int_{-h_{\rm ml}}^{0} \mathbf{u}\, dz$, which corresponds to the latter two terms in Eq. (2) by continuity]. In this case the mixed layer entrains fluid from below. Here w_e is negative if $\partial h_{\rm ml}/\partial t < -\nabla \cdot \mathbf{U}$. In this case the mixed layer re-forms at a depth that is shallower than what would result from upwelling only and detrainment takes place (e.g., de Ruijter 1983). By this process well-mixed water becomes part of the thermocline.

In the kinematical approach this relation [Eq. (2)] is used to determine subduction. We will follow the usual convention to define a detrainment rate [sometimes called the instantaneous subduction rate, e.g., Cushman Roisin (1987), Marshall et al. (1993)]:

$$S_{\rm kin} = -w_e \quad \text{if } w_e < 0. \tag{3}$$

If $w_e > 0$, $S_{\rm kin}$ can be regarded as the entrainment rate.

A natural way to determine the annual subduction as defined in section 1 is to follow a water column for one year and monitor the changes in mixed layer depth by entrainment and detrainment or Eq. (3) (Woods and Barkman 1986; Qiu and Huang 1995). However, it is computationally expensive to analyze Eq. (3) in a Lagrangian framework, especially when the horizontal resolution is high. An alternative is to estimate the subduction rate from the annual volume flux across the deepest winter mixed layer base (Marshall et al. 1993). If there is no interannual variability, the annual mean subduction rate by the mean flow can be approximated by

$$S_{\rm anm} = -(\overline{\mathbf{u}}_w \cdot \nabla h_w + \overline{w}_w). \tag{4}$$

Here h_w is the deepest mixed layer depth in the winter and $\overline{\mathbf{u}}_w = (\overline{u}_w, \overline{v}_w)$ and $\overline{w}_w$ are the annual mean horizontal and vertical velocities at the deepest mixed layer base. We define an annual subduction rate as $S_{\rm ann} = S_{\rm anm} \times \mathcal{T}_{\rm yr}$, with $\mathcal{T}_{\rm yr}$ the number of seconds in a year. Note that $S_{\rm ann}$ is defined as subduction if $S_{\rm ann}$ is positive. If it is negative it can be defined as obduction (Qiu and Huang 1995). This approximation is the result of a linearization around the deepest mixed layer base of a water column at two consecutive winters (see Marshall and Marshall 1995). The first term on the right-hand side is called the lateral induction. It is the annual mean horizontal mass transport through an arbitrarily defined interface that is constant in time. In this case, we determine the transport through the interface spanned by the deepest mixed layer base. This reflects the so-called ''Stommel's mixed layer demon'' (e.g., Marshall et al. 1993). Due to the seasonal cycle in entrainment/detrainment, only water is subducted that detrains just after the mixed layer has reached it deepest level. Water that detrains later in the year will not escape deepening of the mixed layer by reentrainment. So the properties of the subducted water are biased to late winter properties.

Note that the annual average of Eq. (2) is not equal to Eq. (4). In Eq. (2) the advection term (partly) compensates the local thickness tendency. It is not associated with a transport through the mixed layer base [see also Marshall and Marshall (1995) for a discussion on this issue]. The difference between Eqs. (2) and (4) reflects the difference between the net annual detrainment/entrainment and subduction/obduction.

A simple annual mean of $S_{\rm kin}$ results in an annual-mean detrainment (entrainment) rate, which is different from the annual subduction (obduction) rate because the interface $h_{\rm ml}$ varies in time in contrast to h_w. It should also be noted that the subduction rate according to Eq. (4) is not equal to the subduction rate defined in a Lagrangian framework. In Eq. (4) the along-trajectory changes and seasonal changes are neglected. This leads, in general, to inflated values near mixed layer fronts (Qiu and Huang 1995).

The lateral induction, the vertical velocity, and the annual subduction rate ($S_{\rm ann}$) into the mode water layer following Eq. (4) are shown in Fig. 4 for experiment 1. In the entire subtropical region, the deepest mixed layer depths are reached in March. The annual mean velocities in the mode water layer at the outcrop position in March are used to determine the lateral induction. The vertical velocity is not explicitly defined in isopycnic models. It is diagnosed by using the continuity equation: $h_w^{-1} \int_{-h_w}^{0} \nabla_h \cdot \mathbf{u} h\, dz = w_w$.

The patterns and amplitudes resemble estimates of annual subduction rates deduced from observations. Marshall et al. (1993) found subduction rates up to 150 m yr^{-1} using a highly smoothed dataset (Marshall et al. 1998). Using tritium-age observations, Jenkins (1988) estimated subduction rates of 80 m yr^{-1} at the northeastern part of the gyre. In our model the annual subduction rate is 100 m yr^{-1} there. These results show that despite the simple configuration of the model, these physical processes have the same order of magnitude in the present model as in the observations. But, care must be taken, and these absolute numbers should be verified in a realistic context.

Mode water is formed just south of the Gulf Stream extension. The process starts in the east due to the difference in seasonal cycle between the eastern part and the western part of the gyre: the outcrops (not shown) in late winter are deflected to the south on the eastern side of the gyre. In spring they move rapidly to the north responding to the seasonal cycle in the forcing. This causes a large heat gain in the mixed layer. On the western side, advection of warm water in the western boundary current dominates, which results in a small seasonal cycle in the position of the outcrops.

South of the Gulf Stream extension the winter mixed layer slopes upward toward the south and the mean flow is directed to the south (see section 3). This results in large values of the lateral induction term. The negative vertical velocity is mainly due to downward Ekman pumping in the gyre. The mode water is reentrained (obducted) in the western boundary current region. Here lateral induction dominates.

As the model domain is small and the flow strong,

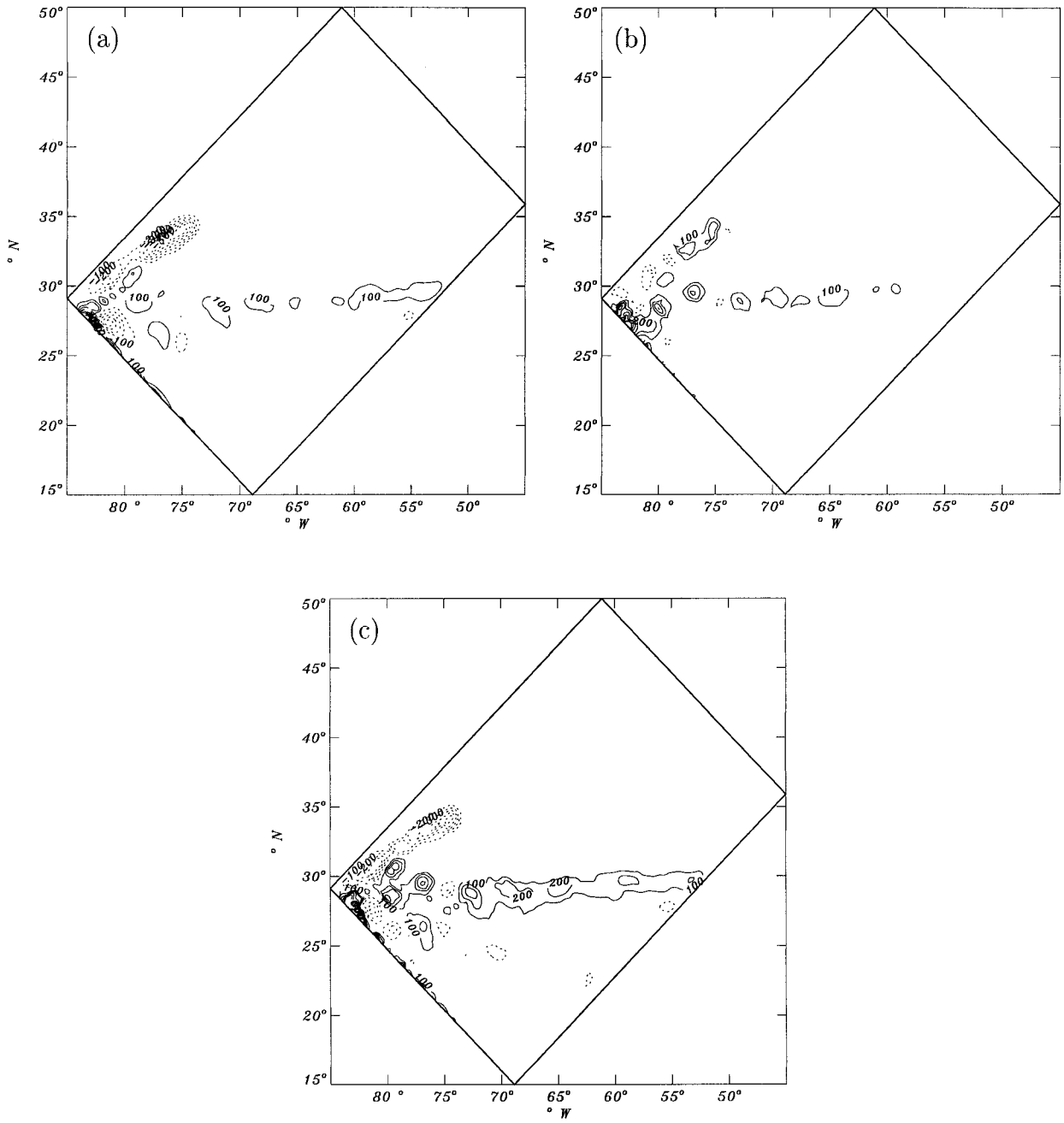

FIG. 4. (a) Annual lateral induction, $-\overline{\mathbf{u}}_w \cdot \nabla h_w$ (m yr^{-1}), from the mixed layer into mode water for expt 1; (b) annual vertical velocity, $-w_w$ (m yr^{-1}), into mode water; and (c) the annual subduction rate, S_{ann} (m yr^{-1}), into mode water. Positive values imply a positive contribution to the mode water volume. Only the contribution by the mean flow is depicted.

the time for a water parcel to propagate from the region where it is subducted to the region where it is reentrained can be less than 360 days. However, due to the shortening of the seasonal cycle (see section 2) 360 days are equivalent to three seasonal cycles. On the average, it takes two to three seasonal cycles for a water parcel to travel from the main subduction region (around 28°N, 70°W) to the upwelling region in the Gulf Stream.

The annual subduction is defined as the integral of the annual subduction rates over the region where subduction occurs, that is, the integral of the positive numbers in Fig. 4c. A total subduction of 5.2 Sv is found. Realistic ocean models show slightly higher amounts of subduction [e.g., Marsh and New (1996) found 6 Sv]. However, subduction rates were somewhat lower [O(100 m yr^{-1})]. Therefore, the difference in subduction may be attributed to the small outcrop regions due to the small idealized domain of the present model. Com-

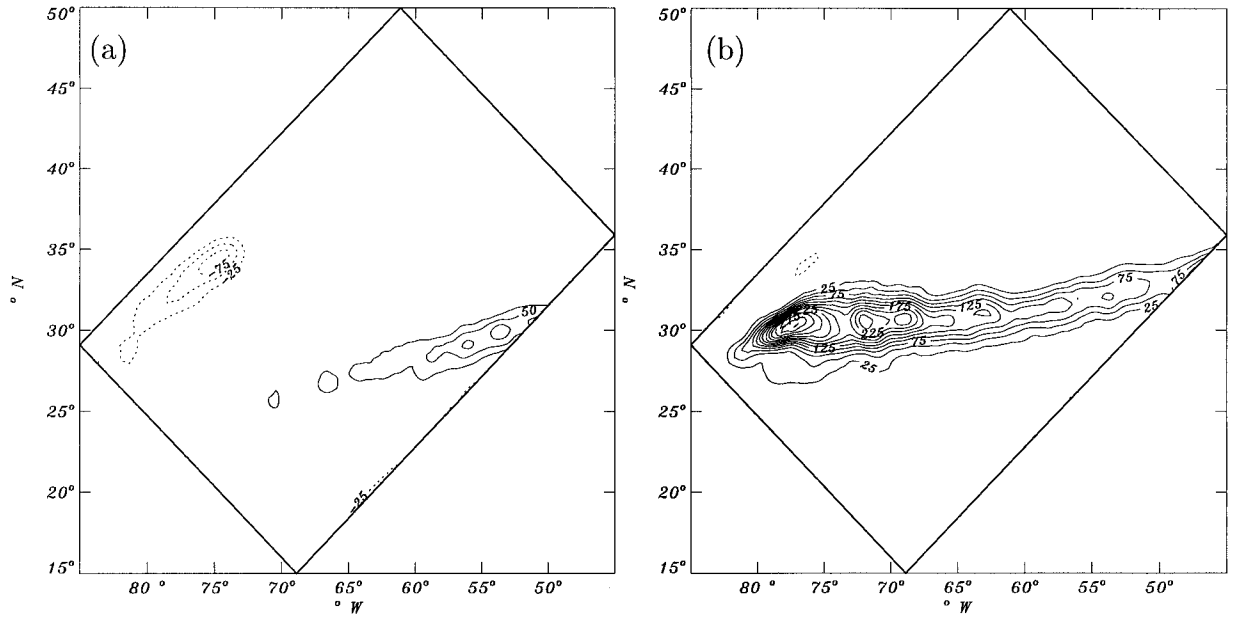

FIG. 5. (a) Monthly integrated entrainment/detrainment rates (m month^{-1}) from the mixed layer into the mode water layer in expt 1. (a) Mar and (b) May. Positive values mean a positive contribution to the thickness budget of the mode water layer.

parable patterns and amplitudes were found for experiment 2. However, the maximum mixed layer depth occurs in the month February in experiment 2 instead of March. The patterns of subduction in experiment 1 and 2 are not compared as the mixed layer front lies more to the south in February. The total subduction was 2 Sv less in experiment 2.

The flow and stratification in both model versions is different (see section 2). The differences in subduction by the mean flow can be due to differences in the mean flow or due to analyzing at a different grid. That is, when analyzing the same dataset at a coarser grid, gradients become less sharp and the diagnosed subduction may be reduced merely due to the resolution of sampling. To estimate the sampling effect, the subduction in experiment 1 was determined from velocities and thicknesses extrapolated to the coarser grid (74 km). Although the gradients became less sharp the subduction was reduced only by 0.2 Sv. Therefore, the differences should be attributed to the presence of eddies in experiment 1. They are caused by an eddy-induced change in the mean flow, which on its turn, results from the reduced horizontal diffusion and increased horizontal resolution.

b. Eddy contribution to subduction

The contribution of eddies to the annual subduction rate cannot be estimated by decomposing the velocity and thickness in mean and eddy components in Eq. (4). No eddy correlations arise because subduction through the sloping interface h_w is considered, which is constant in time; that is, h_w' is not defined (see also Marshall 1997). To determine the total (and eddy) subduction another procedure has to be followed. One way would be to interpolate $-(\mathbf{u} \cdot \nabla h + w)$ at h_w for every time step. Due to archiving limitations this is not possible without several simplifying assumptions. Alternatively, one can determine the total fluxes by integrating the instantaneous detrainment rates [Eq. (3)] during the period in which fluid that is detrained to the mode water layer escapes irreversibly to the main thermocline. This defines the *effective* subduction period, $\mathcal{T}_{\text{ef}}$, (e.g., Marshall et al. 1993); that is,

$$S_{\text{tot}} = \int_{\mathcal{T}_0}^{\mathcal{T}_0+\mathcal{T}_{\text{ef}}} S_{\text{kin}}\, dt, \tag{5}$$

where S_{tot} is the total subduction (mean plus eddy components). Detrainment ($S_{\text{kin}} > 0$) of the mixed layer starts in March ($\mathcal{T}_0$), after the mixed layer has reached its deepest level, and continues until midsummer. A part of the detrained water is reentrained in the same year during fall or winter. The remaining part defines the water that is subducted. In spring, the detrainment rate is maximal as warming causes the mixed layer to restratify. Detrainment starts in March at the northeastern side of the gyre (see Fig. 5). During spring the region of net monthly detrainment extends to the west. In May detrainment rates into mode water are maximal. Note that most of this water will be reentrained and does not contribute to the annual subduction. Values in Fig. 5b are much larger compared to Fig. 4c. It can already be seen from this figure that the effective subduction, $\mathcal{T}_{\text{ef}}$, period will be shorter than 3 months. So, we define $\mathcal{T}_{\text{ef}}$ as the period from March on, in which the flow detrains

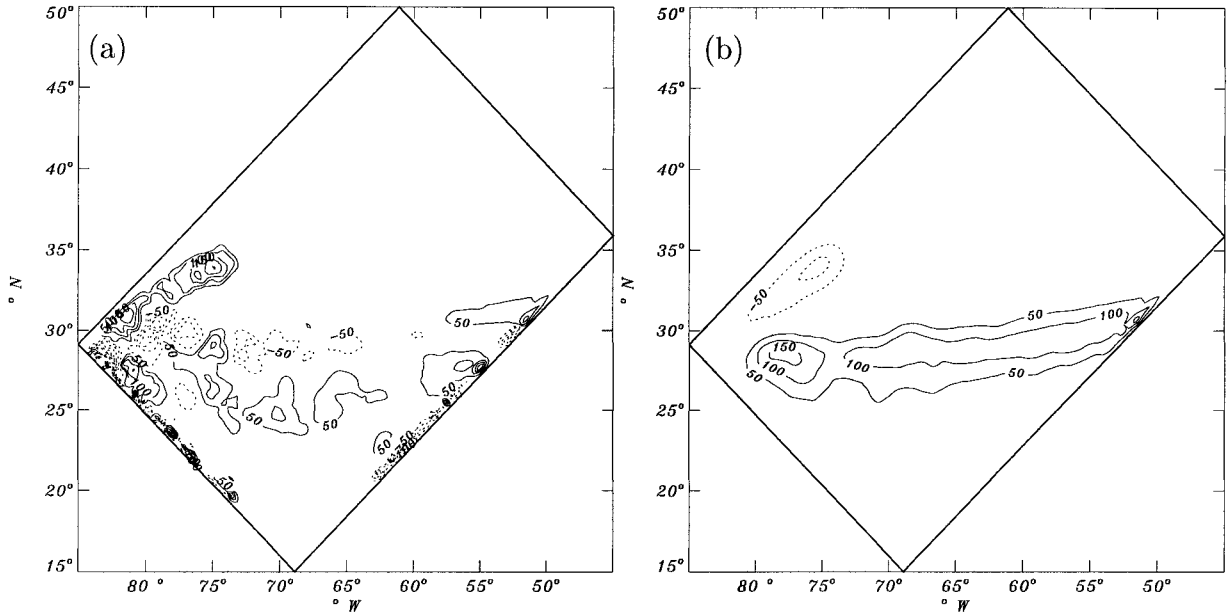

FIG. 6. (a) Eddy subduction rate (m yr^{-1}) into the mode water layer. (b) Total subduction rate (m yr^{-1}) into mode water. Positive values mean a positive contribution to the mode water volume.

the same amount of water as is annually subducted by the flow. After $\mathcal{T}_{ef}$ all the water that is detrained will be reentrained (elsewhere) in the mixed layer within the same seasonal cycle, that is, at the onset of the winter when the mixed layer deepens.

To determine $\mathcal{T}_{ef}$, the basin-integrated S_{tot} must be known exactly. The S_{tot} can only be estimated with a few simplifying assumptions, as we lack all the data to calculate this number exactly. As a test for the simplifications we will make, we will first calculate S_{ann} for the mean flow according to Eqs. (4) and (6), estimating $\mathcal{T}_{ef}$ for the mean fields only:

$$S_{ann} = -\int_{\mathcal{T}_0}^{\mathcal{T}_0+\mathcal{T}_{ef}} \left(\frac{\partial h^*_{ml}}{\partial t} + \mathbf{u}^*_{ml} \cdot \nabla h^*_{ml} + w^*_{ml} \right) dt. \quad (6)$$

For any variable x, x^* stands for the monthly mean of x. Using Eq. (6), and we find $\mathcal{T}_{ef} = 1.8$ months. In general, by neglecting eddy effects we will underestimate $\mathcal{T}_{ef}$ by restricting ourselves to the subduction by the mean flow (assuming that the eddies enhance the annual mean subduction). An estimate for $\mathcal{T}_{ef}$ for the total flow can be obtained by calculating S_{tot} according to the interpolation procedure described in the beginning of this section. To do so, we have to assume that on the long-term $\nabla \cdot (\mathbf{u}h)$ in the mixed layer is compensated by $\nabla \cdot (\mathbf{u}h)$ in the underlying isopycnic layer. This is reasonable as, apart from the small mass exchange due to diapycnal diffusion, there is only a mass exchange possible between the mixed layer and the outcropping layer. From the monthly mean fields we estimate h_w and the density of the underlying layer. By linear interpolation and assuming the compensation effect described above, $\nabla \cdot (\mathbf{u}h)$ at h_w is estimated from the 3-day averages of $\nabla \cdot (\mathbf{u}h)$ at the bottom of the mixed layer. Following this procedure, we estimate $\mathcal{T}_{ef} = 2.2$ months for the total flow. Both estimates for $\mathcal{T}_{ef}$ (1.8 and 2.2 months) closely resemble each other. The slightly larger $\mathcal{T}_{ef}$ obtained for the total fields is consistent with the assumption that the eddies enhance $\mathcal{T}_{ef}$. As our method to determine $\mathcal{T}_{ef}$ is not exact, we will use $\mathcal{T}_{ef} = 2$ months in the remaining of this paper. This number corresponds well with estimates made by Marshall et al. (1993). They found an effective subduction period of 1 to 3 months south of the Gulf Stream extension. This shows that, at first order, the subduction acts on the same timescale as in the observations. The short period implies that subducted fluid is biased to late winter properties (Stommel's mixed layer demon).

We deduce the total annual subduction into mode water, including the contribution of the time-varying flow (eddies), from the integral of the instantaneous detrainment rates over the effective subduction period using Eq. (5). The mean subduction has been presented in 4a. To determine the contribution of eddies correctly, the mean fields consist of monthly means that contain the seasonal cycle. If $\mathcal{T}_{ef}$ is estimated correctly, this method is equivalent to the method described by Marshall [1997, his Eq. (12)]. Moreover, by comparing the local subduction rates obtained by Eq. (5) and by the interpolation method described above, we can check whether the latter gives a good estimate. Comparing both patterns, it appears that the differences are generally less than 10% (not shown), which confirms that our estimate of $\mathcal{T}_{ef}$ is adequate.

Figure 6 shows the total and eddy subduction. The

pattern of eddy subduction is rather noisy, but an independent analysis of the first 10 years and the last 9 years of the simulation resulted in virtually the same patterns and magnitudes. Away from the boundary current, eddies enhance subduction near 25°N. Here the total subduction is dominated by the eddy contribution. Eddies reduce subduction rates to the north of this line, in the region where most subduction by the mean flow occurs. In the western boundary current region the eddies reduce reentrainment or obduction. So the eddy contribution counteracts the subduction/obduction by the mean flow at most places. The amplitude of the eddy contribution as obtained from the pattern in Fig. 6a (only positive numbers) is somewhat lower, but of the same order of magnitude as the annual mean subduction, that is, 2.5 Sv compared to 5.2 Sv (for $\mathcal{T}_{ef} = 1.8$ months we found 2.4 Sv and for $\mathcal{T}_{ef} = 2.2$ months we obtain 2.6 Sv, hence showing that results are not very sensitive to small differences in the effective subduction period). The difference between the total subduction estimated from Fig. 6b and the subduction by the mean flow (Fig. 4c) is 2 Sv.

5. Net annual entrainment and detrainment

A mass flux through the mixed layer base into or from the thermocline is only possible by deepening/shoaling of the mixed layer by entrainment/detrainment. Generally, net formation of a water mass by a net detrainment takes place at a different latitude than entrainment of the water mass into the mixed layer. This implies a zonally averaged vertical overturning (in density space). The overturning is sometimes referred to as the shallow Ekman overturning. The corresponding transport of mass is equivalent to a transport of heat. So, there is a meridional heat transport associated with the net mass exchange by entrainment/detrainment.

The annual mean of entrainment/detrainment rates differs from annual subduction. The mass exchange by entrainment/detrainment of the mixed layer takes place over the entire seasonally varying outcrop at the moving mixed layer base. Subduction takes place only at the end of the winter or early spring at the deepest winter mixed layer base. After subduction has ceased, detrainment may go on but the detrained fluid will be reentrained later in the same year elsewhere. In this case, the net annual detrainment will be larger than the annual subduction. Also, after subduction has ceased, entrainment may dominate detrainment. In that case, the net annual detrainment will be less than the annual subduction. These differences have been pointed out in detail by Marshall and Marshall (1995, their section 4). The results presented here will confirm their conclusion, that annual subduction differs from the annual mean of entrainment/detrainment.

In this section we will evaluate the net entrainment/detrainment. In the numerical model, the mass fluxes by entrainment and detrainment are unambiguously defined. Therefore the layer thickness equation is used to diagnose entrainment and detrainment rates. Within the numerical model this is most appropriate, as the individual terms of the model equation represent the different physical processes. A closed budget can be derived for the layer thickness equation.

a. Thickness budget

In isopycnic models the continuity equation is applied to a homogeneous volume of water between two isopycnal surfaces. This results in a prognostic equation for isopycnic layer thickness. In the numerical model various sources and sinks are added to this equation, which leads to the following equation for isopycnic layer thickness:

$$\frac{\partial h}{\partial t} = -\nabla \cdot (\mathbf{u}h) + \mathcal{W} + \mathcal{D} + \mathcal{S}, \tag{7}$$

where $\nabla = \partial/\partial x + \partial/\partial y$, h is the layer thickness, $\mathbf{u} = (u, v)$ is the horizontal velocity, $\mathcal{W}$ is the lateral (isopycnal) diffusion of layer thickness, $\mathcal{D}$ is the advective transport associated with the diapycnal diffusion, and $\mathcal{S}$ is a source term that comprises mass fluxes across the base of the mixed layer due to deepening/shoaling of the mixed layer by entrainment/detrainment. The same equation is applied to the mixed layer thickness, but the advective transport due to diapycnal diffusion is omitted there. This turbulent flux is already included in the mass fluxes associated with entrainment and detrainment.

When applied to the mixed layer, the entrainment/detrainment rate in the layer thickness equation [Eq. (7)] is almost equivalent to the entrainment velocity described in the previous section [i.e., Eqs. (2) and (3)]. In Eq. (7) the vertical velocity at the base of the mixed layer is not included explicitly, as the advection term is written in the flux form. However, it can be split into

$$\nabla \cdot (\mathbf{u}h) = \mathbf{u} \cdot \nabla h + h\nabla_h \cdot \mathbf{u}. \tag{8}$$

The last term yields the vertical velocity at the base of the mixed layer by continuity and the rigid-lid assumption. In the isopycnic model, the equations are applied to discrete layers. So h, u, v are layer variables. There is a discontinuity at the layer interfaces. To make the kinematical theory as presented in section 4a, especially Eq. (2), compatible with the slab mixed layer formulation in the numerical model, we replace $\mathbf{u}_{mb}$ by $\mathbf{u}_{ml}$ in Eq. (3). In that case:

$$\mathcal{S}_{ml} = -S_{kin} - (\mathcal{W} + \mathcal{D}). \tag{9}$$

Here ml stands for mixed layer. Apart from the $\mathcal{W} + \mathcal{D}$, which will be shown to be small, the detrainment rate S_{kin} is equivalent to the detrainment rate in the model. When $\mathcal{S}_{ml}$ is positive: $\mathcal{S}_{ml} = w_e$ [see Eq. (3)].

When studying mode-water formation in the numerical model it is straightforward to determine the net annual mass flux into the mode water from the thickness equation for the mode water layer instead of the mixed

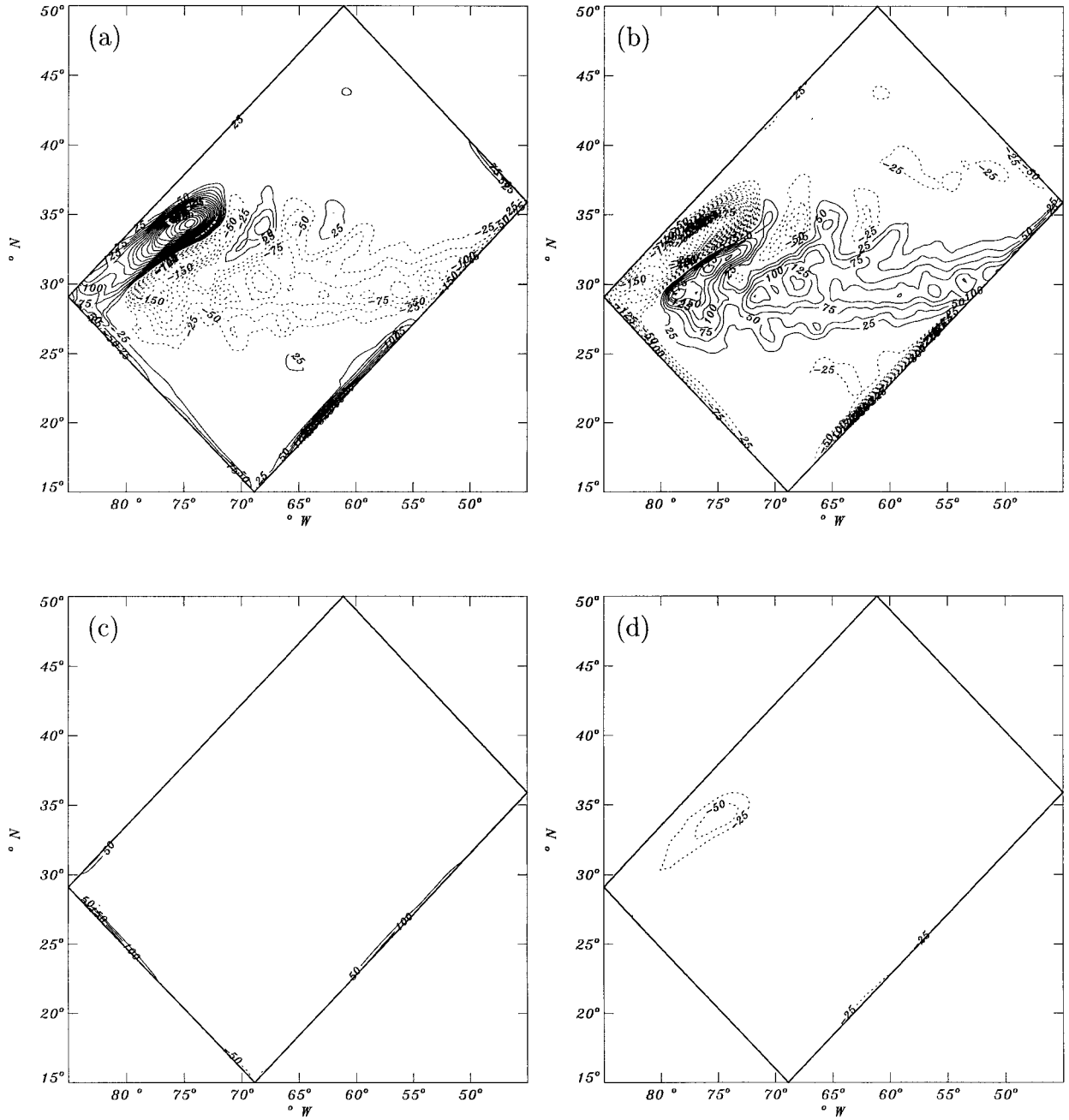

FIG. 7. The contribution of the terms in the thickness budget for the mode water layer [see Eq. (7)]. (a) The lateral advection $-\nabla \cdot (\mathbf{u}h)$ in the mode water layer, (b) the mass flux from the mixed layer to the mode water layer ($\mathcal{S}$), (c) the mass flux due to lateral diffusion and diapycnal diffusion ($-\mathcal{W} - \mathcal{D}$), and (d) the thickness tendency $\partial h/\partial t$. All values are expressed in meters per year.

layer. The horizontal distribution of each of the terms in Eq. (7) for the mode water layer is shown in Fig. 7. The contributions are determined by integrating the contributions of each term over the 19 seasonal cycles. Clearly, the time-integrated mass flux through the base of the mixed layer due to deepening/shoaling of the mixed layer by entrainment/detrainment ($\mathcal{S}$) is balanced by the time-integrated lateral advection of mass [$\nabla \cdot (\mathbf{u}h)$] in the mode water layer. Diffusion ($\mathcal{W} + \mathcal{D}$) hardly contributes to the time-averaged thickness budget. There is a small drift indicated by the loss of mass in the western boundary current region. So, integrated over a long time:

$$\int_T \mathcal{S}\, dt \approx \int_T \nabla \cdot (\mathbf{u}h)\, dt. \tag{10}$$

Note that this integration comprises both the contribu-

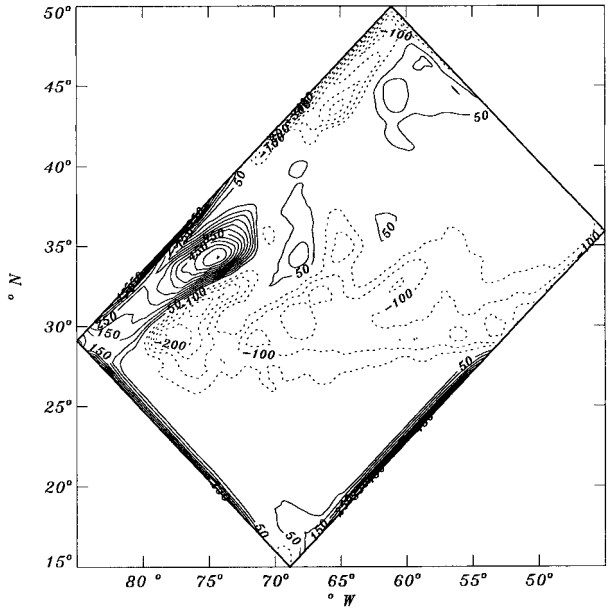

FIG. 8. (a) Annual mass flux due to entrainment/detrainment (m yr^{-1}) from interior layers to the mixed layer.

tions of the eddies and the mean flow. The time T over which $\mathcal{S}$ is integrated must resolve a number of seasonal cycles in order to neglect the thickness tendency. A balance as in Eq. (10) is valid for all layers in the upper thermocline, including the mixed layer.

In Fig. 7b, a positive annual mass flux implies a net transfer of fluid from the mixed layer into the mode water layer. Figure 8 shows the horizontal distribution of the time-integrated $\mathcal{S}_{\text{ml}}$. Indeed, Figs. 7b and 8 show that the mode water is formed (eroded) where the mixed layer shoals by detrainment (deepens by entrainment) south of the 18°C outcrop. Figures 7b and 8 are nearly the opposite south of 38°N where the 18°C layer outcrops. The high mass fluxes in the northwestern corner of the basin in Fig. 8 are related mainly to formation and eroding of the 6°C layer.

The large net detrainment rates just south of the Gulf Stream extension (between 25°N and 35°N) are caused by the large seasonal variation of the mixed layer depth in this region. Also the convergence of the horizontal transport is large in this region. In a statistically steady state, the convergence of the horizontal transport balances the mass flux through the base of the mixed layer due to entrainment/detrainment. In a statistically steady state isopycnic layers do not inflate. Net detrainment rates at one place must be balanced by net entrainment somewhere else. The reentrainment process (upwelling trough the base of the mixed layer) takes place mainly in the western boundary current. There is localized upwelling on the eastern boundary due to the wind forcing and the presence of a solid wall. Furthermore, localized upwelling takes place in northward excursions of the Gulf Stream meanders (Figs. 7b, 8).

The annual net detrainment in a specific water mass is defined as the integral of the net detrainment rates (after one or a number of seasonal cycles) multiplied by the area over which the detrainment takes place. For the mode water layer this results in a net detrainment of 5.6 Sv.

b. Eddy mass flux in a ventilated layer

Formation of a water mass by detrainment is only possible at places where a water mass is in contact with the mixed layer, that is, at the outcrops. Due to eddy motions the outcrops meander. This leads to SST anomalies and, consequently, anomalous surface heat fluxes. Also, the stratification of the water column is affected by the eddy motions. This will also affect entrainment and detrainment rates. The varying entrainment and detrainment rates, and the varying outcrop areas, give rise to an eddy mass flux from the mixed layer into interior layers. The eddy contribution to the net annual detrainment/entrainment can be directly calculated from the thickness budget of the mode water layer.

The total lateral transport, $\mathbf{u}h$, in an isopycnic layer of the eddy-resolving model can be separated in a mean ($\overline{\mathbf{u}}\overline{h}$) and an eddy contribution ($\overline{\mathbf{u}'h'}$). The mean values are determined from the monthly means such that the mean transport comprises the seasonal cycle.

We can define an eddy transfer velocity $\overline{\mathbf{u}'h'}/\overline{h} = \mathbf{u}_*$ in addition to the mean velocity, $\overline{\mathbf{u}}$. The eddy transport is related to entrainment and detrainment rates according to

$$\mathcal{S}_{\text{tot}} = \int_T (\mathcal{S}_{\text{mean}} + \mathcal{S}_{\text{eddy}})\, dt$$

$$\approx \int_T (\boldsymbol{\nabla} \cdot (\overline{\mathbf{u}}\,\overline{h})_{18} + \boldsymbol{\nabla} \cdot (\overline{\mathbf{u}'h'})_{18})\, dt \qquad (11)$$

$$= \int_T (\boldsymbol{\nabla} \cdot (\overline{\mathbf{u}}\,\overline{h})_{18} + \boldsymbol{\nabla} \cdot (\mathbf{u}_*\overline{h})_{18})\, dt. \qquad (12)$$

Here $\mathcal{S}_{\text{eddy}}$ stands for the eddy contribution to the mass flux from the mixed layer to the mode water layer.

Figure 9 shows the horizontal distribution of the divergence of the eddy transport in mode water $[\boldsymbol{\nabla} \cdot (\mathbf{u}_*\overline{h})]$. The amplitudes are highest in regions of high baroclinic activity, that is, in the Gulf Stream, the Gulf Stream extension, and the westward return flow of the subtropical gyre. In the Gulf Stream the patterns are not single signed. In the westward return flow (along 27°N) the divergence of the eddy transport is uniformly positive.

The annual contribution of the eddy mass flux in the mode water layer in the balance of Eq. (7) can be derived from Fig. 9. It is 1.9 Sv compared to a total net detrainment of 5.6 Sv. In section 6 we will compare these results with the subduction rates found in 4b.

The mean flow in the fine-resolution model (experiment 1) differs from the mean flow in the coarse-res-

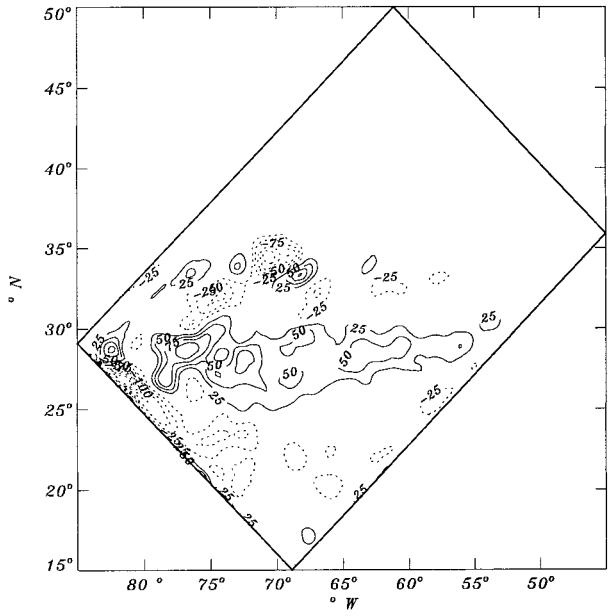

FIG. 9. Divergence of the eddy transport $[\nabla \cdot (\overline{\mathbf{u}'h'}) = \nabla(\mathbf{u}_* \overline{h})]$ in the mode water layer expressed in meters per year.

olution model (experiment 2). The model formulations, however, differ only in the horizontal resolution and the friction and diffusion parameterization. In both experiments diffusion is not dominant in the layer thickness budgets. So, the different detrainment/entrainment rates by the mean flow in the fine resolution compared to the coarse resolution version of the model is due to a rectification of the mean flow by its instabilities. We will call this the *eddy-induced part of the mean flow*. Together with the eddy contribution itself $[\nabla \cdot (\mathbf{u}_* \overline{h})]$, the contribution by the eddy-induced part of the mean flow adds up to the eddy-induced change in detrainment/entrainment. In a statistically steady state, the eddy-induced change in detrainment/entrainment, $\Delta\mathcal{S}$ is (diffusion is neglected):

$$\Delta\mathcal{S} = \nabla \cdot [\overline{(\mathbf{u}h)}_1 - \overline{(\mathbf{u}h)}_2]$$

$$= \nabla \cdot (\mathbf{u}_* \overline{h}) + \nabla \cdot [(\overline{\mathbf{u}}\,\overline{h})_1 - (\overline{\mathbf{u}}\,\overline{h})_2] \quad (13)$$

$$= \nabla \cdot (\mathbf{u}_* \overline{h}) + \Delta Q. \quad (14)$$

Here ΔQ is the eddy-induced part of the mean flow, the subscripts 1, 2 stand for the respective experiments. The zonally integrated eddy mass flux itself $[\int \nabla \cdot (\mathbf{u}_* \overline{h})\, dx]$ compensates the zonally integrated eddy-induced part of the mean flow $(\int \Delta Q\, dx)$ when the thermal driving is weak (e.g., weak restoring time constant in the surface heat flux parameterization). In that case, the total mass fluxes in the high-resolution model will be the same as in the low resolution model; that is, $\int \Delta\mathcal{S}\, dx = 0$ (e.g., Cox 1985; Böning and Budich 1992). When the thermal driving is strong, the eddy-induced part of the mean flow can be rearranged such that compensation no longer takes place (Drijfhout 1994b); that is, $\int \nabla \cdot (\mathbf{u}_* \overline{h})\, dx \neq \int \Delta Q\, dx$. In the present model no compensation takes place because the thermal driving is strong on the eddy scale [see Drijfhout and Walsteijn (1998) for a detailed evaluation]. This is also reflected in the different eddy contributions presented below.

The eddy-induced change in entrainment/detrainment rates ($\Delta\mathcal{S}$) is depicted in Fig. 10. High values are found in the western boundary current. The basin-integrated eddy-induced mass flux into mode water obtained from the pattern in Fig. 10a is 2.3 Sv. Figure 10b shows the difference between the eddy-induced change in entrainment/detrainment and the eddy contribution derived from the eddy fluxes, that is, $\Delta\mathcal{S} - \nabla \cdot (\mathbf{u}_* \overline{h}) = \Delta Q$ [note that Fig. 10b is equal to Fig. 10a minus Fig. 9, see also, Eq. (14)]. This change in net entrainment/detrainment by the eddy-induced part of the mean flow is 2.7 Sv. Figures 10c and 10d show the change in velocity and thickness, or volume transport, in the mode water layer by the eddy-induced part of the mean flow (ΔQ). The changes are largest in the western boundary current region. Also, the effect of the standing wave in the midlatitude jet is visible. This standing wave is absent in experiment 2. The change in volume transport converges toward the inflow of the western boundary current and diverges at the outflow of the boundary current. This volume transport by the eddy-induced part of the mean flow (ΔQ) forces the total eddy-induced change in entrainment/detrainment rates ($\Delta\mathcal{S}$) in Fig. 10a.

The eddy mass flux itself in the ventilated layer $[\nabla \cdot (\mathbf{u}_* \overline{h})]$ is confined to the midlatitude jet-recirculation area (Fig. 9). The mass fluxes by the eddy-induced part of the mean flow (ΔQ) are large in the tight recirculation in the west where the western boundary current leaves the coast (Fig. 10b). This difference shows that compensation does not take place everywhere. In the midlatitude jet and the recirculation area, the zonally integrated eddy mass flux itself and the eddy-induced change in the mass fluxes nearly compensate:

$$\int [\nabla \cdot (\mathbf{u}_* \overline{h}) + \Delta Q]\, dx \approx 0.$$

In the western boundary current region there is no compensation. This is reflected by the large values of the total eddy-induced mass fluxes ($\Delta\mathcal{S}$, Fig. 10a).

In general, $\Delta\mathcal{S}$ is dominated by the contribution of the eddy-induced part of the mean flow, $\int \Delta Q\, dx$ (Fig. 10a and Fig. 10b are similar). The dominance of ΔQ compared to $\nabla \cdot (\mathbf{u}_* \overline{h})$ can be understood from the thermal driving. The damping of SST anomalies depends on the spatial scale of the anomalies. Smaller anomalies are more strongly damped. The damping is stronger on the eddy scale than on the larger scale of the eddy-induced part of the mean flow (see Drijfhout and Walsteijn 1998). This stronger damping on the eddy scale affects the mass fluxes associated with en-

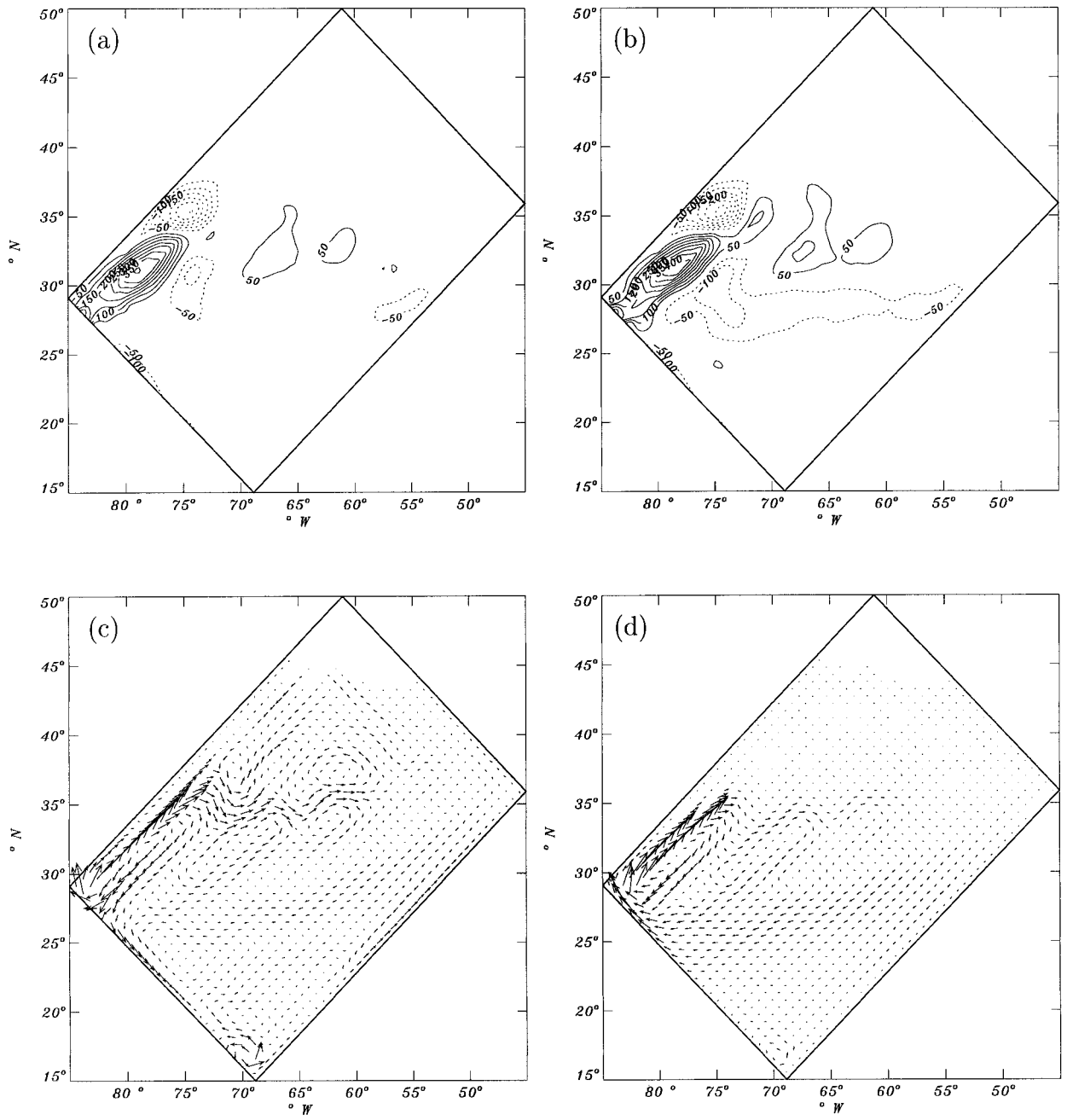

FIG. 10. (a) Eddy-induced change in entrainment/detrainment rates into mode water [ΔS, see Eq. (14)], i.e., difference between eddy-resolving and coarse-resolution run (m yr^{-1}). (b) Change in entrainment/detrainment into the mode water layer by the eddy-induced change of the mean flow (ΔQ). (c) Change in velocity in mode water by eddy-induced part of mean flow (largest vector corresponds to 0.6 m s^{-1}). (d) Change in thickness transport in mode water by eddy-induced part of the mean flow (largest vector corresponds to 77 m^2 s^{-1}).

trainment/detrainment. It explains why the detrainment by the eddy-induced part of the mean flow (ΔQ) dominates the eddy mass flux itself [$\nabla \cdot (\mathbf{u}_* \overline{h})$]. The basin-integrated enhancement by the eddies in net annual detrainment is somewhat less than 2.3 Sv because part of the eddy-induced change counteracts the detrainment of the mean flow in the coarse-resolution run. The enhancement is 1.8 Sv, that is, experiment 1 yields 5.6 Sv and experiment 2 yields 3.8 Sv.

6. Discussion

The purpose of this section is to reconcile the results presented in the previous sections. Also, we present a

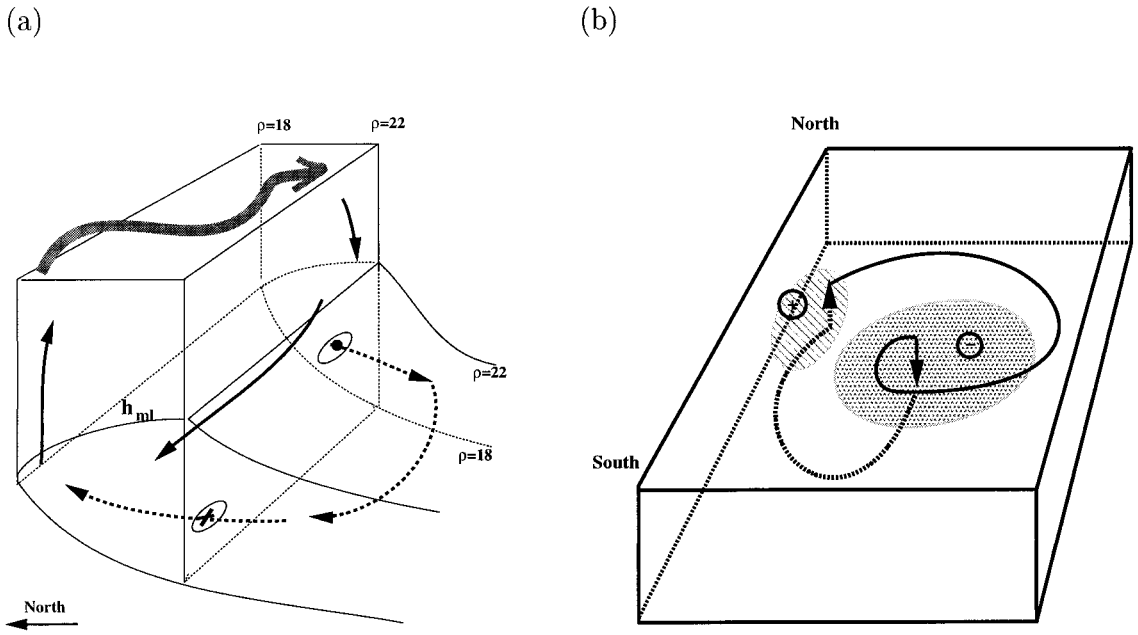

FIG. 11. (a) Schematic drawing of two pathways along which detrained water may flow with respect to the southernmost outcrop: 1) along the directly ventilated region beneath the outcrop (thick lines), or 2) passing through the southernmost outcrop line into the area that is not directly ventilated (dashed lines). The thick gray line symbolizes the meandering flow in the surface layer. (b) Schematic drawing of the pathway of ventilated water. The continuous line shows the pathway in the mixed layer, the dashed line in the ventilated (mode water) layer. The shaded patches correspond to regions of net entrainment and detrainment as in Fig. 7b (see text for details).

picture of the three-dimensional circulation in a ventilated layer in the upper subtropical gyre and discuss the differences with a two-dimensional circulation. Finally we discuss the applicability of the relation between the bolus (or eddy) transport and eddy subduction for a seasonally varying three-dimensional model formulation. Marshall (1997) proposed such a parameterization in a two-dimensional context without seasonal variations.

At the southernmost outcrop water leaves the directly ventilated region (beneath the outcrops) and becomes shielded from the mixed layer and its variations (i.e., $\mathcal{S} = 0$). This is the part of the water that is subducted. Some of the water that passes the southernmost outcrop has been detrained recently, another part is recirculating within the ventilated layer without being entrained or detrained. Also, not all detrained water passes the southernmost outcrop position. The detrained fluid may also flow subsurface along the directly ventilated region to be reentrained in the western boundary current (see Fig. 11a). Note that this picture differs from the two-dimensional picture sketched by Marshall (1997). In the two-dimensional context all detrained water must pass the southernmost outcrop line to retain a steady state. Also, Marshall (1997) did not include a seasonal cycle. In his case, the subtle difference between annual subduction and annual mean detrainment does not exist.

The mass transport across an outcrop line can be quantified using

$$\int_l (\mathbf{u}h)\cdot\mathbf{n}\,dl = \int_l (\overline{\mathbf{u}}\,\overline{h})\cdot\mathbf{n}\,dl + \int_l (\mathbf{u}_*\overline{h})\cdot\mathbf{n}\,dl. \quad (15)$$

Here $\mathbf{n}$ is the unit vector normal to the outcrop line l. So the transport out of the directly ventilated outcrop region can be decomposed in a mean component and an eddy component associated with the bolus transport.

Instead of diagnosing Eq. (15) at an outcrop line, we have determined the transports at a fixed latitude. So the picture is not obscured by the curly outcrop line. The transports in Eq. (15) are determined at 25°N, which is the mean latitude of the southernmost outcrop boundary. This latitude can be taken as reference to study subducted water because nearly all detrainment takes place to the north of this latitude (see Fig. 7b). In the interior part of the gyre the mean flow is directed toward the south (Fig. 12a). The mean southward transport across the outcrop line is 12.5 Sv. On the western side the water flows back into the outcrop area. This is consistent with the mean circulation. The mean transport across 25°N does not exactly balance. The imbalance, however, is small (less than 1 Sv) and can be attributed to drift and the diapycnal mass fluxes south of 25°N. The mean transport across this line is two to three times larger than the annual subduction. This implies that subducted water recirculates on the average two to three times before it is reentrained (obducted) again.

Using Figs. 4, 7b, and 12a, a pathway of ventilated

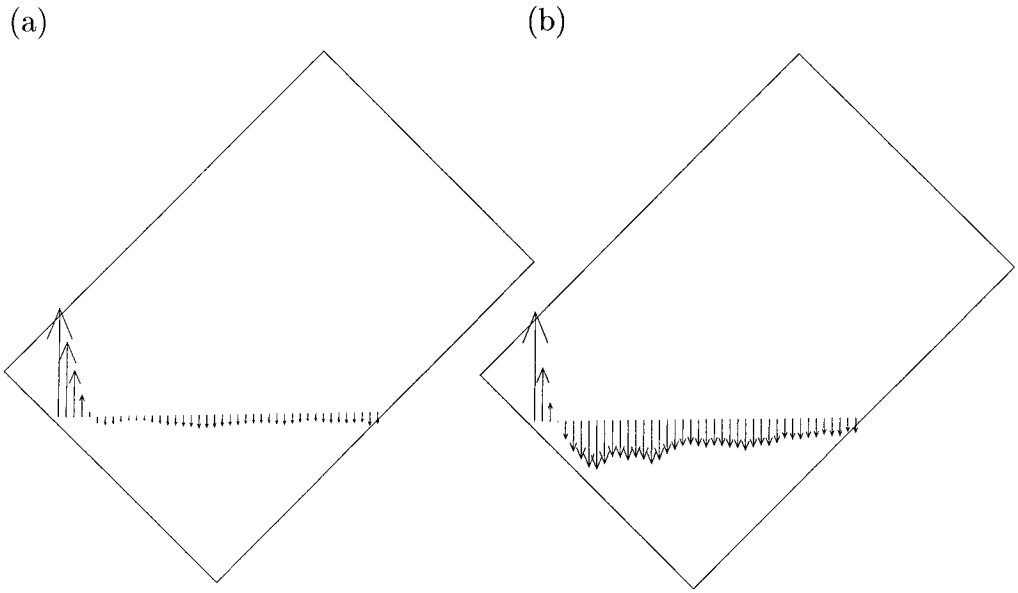

FIG. 12. (a) Mean transports ($\overline{\mathbf{u}h}$) and (b) bolus transport($\mathbf{u}_*\bar{h}$) in the mode water layer through the mean southernmost outcrop of mode water (25°N). Largest vector in (a) corresponds to 46 $m^2\ s^{-1}$, in (b) 4.3 $m^2\ s^{-1}$.

water can be deduced. Detrainment mainly occurs at the southern flank of the midlatitude jet. A part of the detrained water is then advected southward until it joins the westward flowing branch of the subtropical gyre between 20° and 25°N, the model equivalent of the Gulf Stream recirculation. This thermocline water is subducted and flows westward toward the basin boundary where it feeds the northward flowing western boundary current. At the northern flank of the western boundary current/midlatitude jet, just where this current leaves the coast and turns eastward, the subducted thermocline water is reentrained. It joins the surface waters of the midlatitude jet and flows farther eastward. After turning southward and westward within the midlatitude jet–recirculation, it is advected northward within the subtropical gyre toward the southern flank of the midlatitude jet where it is detrained again. This pathway is schematically depicted in Fig. 11b. Note that this is a schematic picture. In reality, diapycnal processes in the mixed layer obscure the pathway in the mixed layer, but on the long-term mean there is a recirculation as depicted in Fig. 11b.

Zonally averaged the mean circulation consists of detrainment (downwelling) at the southern flank of the midlatitude jet, northward advection within the thermocline, entrainment (upwelling) at the northern flank of the midlatitude jet, followed by southward advection within the mixed layer.

The different eddy contributions that have been calculated show that eddies strongly modify the mass flux from the mixed layer to the thermocline. The enhancement of the net entrainment/detrainment by the eddies is the main cause for the increase in the shallow Ekman overturning by eddies discussed in Bryan (1991) and Drijfhout (1994a). This enhanced Ekman overturning partly compensates for the eddy heat transport. The eddy heat transport, associated with the baroclinic instability of the midlatitude jet, tends to flatten the thermocline/mixed layer slope associated with the midlatitude jet front.

The increase in the shallow overturning by the eddies [ΔS, see Eq. (14)] is 1.8 Sv. It arises from a totally different pattern than the eddy mass flux itself [$\nabla \cdot (\mathbf{u}_*\bar{h})$] in the mode water layer. The total eddy-induced changes are confined to the western boundary current region and are dominated by the contribution of the eddy-induced part of the mean flow (ΔQ). The eddy mass flux itself in the mode water layer is highest in the midlatitude jet–recirculation area (see Figs. 10a and 10b).

However, the integrated net increase in the total eddy-induced mass fluxes, the eddy mass fluxes themselves and the eddy contribution to subduction compare favorably (approximately 2 Sv). Also, the bolus transport across the southernmost outcrop has a similar magnitude. The southward bolus transport in the interior (see Fig. 12b) reflects the eddy contribution to the subduction. In the western boundary current the flow returns northward, consistent with the pattern of the eddy mass flux in the ventilated layer. The total southward bolus transport that passes 25°N is 2 Sv. The net bolus transport through 25°N in the mode water layer is southward. This is balanced by eddy-driven upwelling south of 25°N (see Fig. 9). Although the mean transport across the southernmost outcrop and the net entrainment/detrainment do not compare (12.5 Sv compared to 5.6 Sv), the magnitude of the bolus transport does compare with

the total eddy-induced change in subduction and net detrainment.

The different eddy components are a factor 2 to 3 smaller compared to the mean. This is not negligible and the eddy mass fluxes should be parameterized in coarse-resolution ocean models where these processes are not explicitly resolved. In the present model, the different eddy contributions are of a comparable amplitude. Therefore, a parameterization for the eddy contribution to the subduction and net detrainment rate may be related to a parameterization of the bolus transport. Gent and McWilliams (1990) presented a parameterization that has been implemented successfully in coarse-resolution ocean models to parameterize bolus transports in the interior (e.g., Danabosoglu and McWilliams 1995). This study shows that the three-dimensional picture of subduction and net entrainment/detrainment in an eddying ocean is much more complicated than the two-dimensional picture presented by Marshall (1997). It indicates, however, that the parameterization of eddy subduction as proposed by Marshall (1997), which builds upon the Gent and McWilliams eddy-transport parameterization, could be applied in a three-dimensional context.

The amplitude of the eddy subduction may be underestimated due to the relatively coarse resolution of the present model. A further increase of subduction with resolution will be approximately equal to the increase of entrainment/detrainment. The latter can be estimated from the eddy-induced Ekman overturning. It is expected that this overturning will increase at higher resolution as the flow becomes more unstable. On the other hand, the release of available potential energy is limited by the growth rate of instabilities, so the observed basic stratification (steepness of the isopycnals) places an upper bound on the strength of eddy subduction. This is supported by results from Drijfhout 1994a, b in a very similar model. At a resolution of 37 km, the overturning is 2–3 Sv stronger than at 74 km. A further increase of less than 0.5 Sv is found at a resolution of 18 km.

7. Summary and conclusions

The main subduction regions in the subtropical gyre of the North Atlantic coincide with regions of high eddy activity. For example, abundant eddy activity is present in the Gulf Stream region where mode water is formed. The eddies modify the mass flux through the base of the mixed layer. In this study the effect of eddies on subduction and on net entrainment/detrainment on the gyre scale has been addressed in an eddy-resolving and coarse-resolution ocean model. Specific attention has been paid to the formation of mode water, which is the best ventilated layer in the model.

The subduction rates resemble subduction rates deduced from observations. Annual subduction rates into mode water up to 200 m yr^{-1} are found south of the Gulf Stream extension. The timescales and rates of subduction show that, at first order, subduction acts on the same timescale as in the observations. Upwelling through the base of the mixed layer takes place in the western boundary current region. The eddy contribution to the subduction rates are a factor 2 to 3 lower compared to the contribution by the mean flow. In the Gulf Stream region and in the westward return flow of the subtropical gyre, eddy contributions to subduction rates of more than 100 m yr^{-1} are found. These values are comparable with estimates from Follows and Marshall (1994), who found eddy subduction rates of 150 m yr^{-1}. Spall (1995) found similar rates in an idealized model. Enhanced subduction (2 Sv compared to a mean of 5.2 Sv) takes place on the southern side of the wintertime outcrop. To the north of this region subduction is reduced by the eddies. In the western boundary current region reentrainment or obduction is reduced by the eddies.

The net entrainment/detrainment rates into mode water show essentially the same patterns, that is, downwelling through the base of the mixed layer south of the Gulf Stream extension and upwelling through the base of the mixed layer in the western boundary current. It is found that in a statistically steady state the lateral advection of mass balances the mass flux through the base of the mixed layer. For a ventilated layer, the eddy contribution to the entrainment/detrainment can be calculated from the divergence of the eddy thickness transport in that layer. The eddy mass fluxes obtained in this way are consistent with the eddy contribution to the subduction rates. A zonally averaged eddy-driven circulation can be deduced that consists of downwelling at the southern side of the outcrop, near the southernmost outcrop, and upwelling to the north. This cell enhances the shallow Ekman overturning and partly compensates for the eddy heat transport (Drijfhout 1994a). The eddy contribution to the subduction acts in the same direction and has a comparable amplitude as the eddy transport in the ventilated layer. Also, the eddy contribution to the Ekman overturning can be compared to the zonally averaged southward transport across the southernmost outcrop line of the ventilating layers where the increase takes place.

These results imply that the eddy contribution to subduction should be parameterizable by an eddy transport (Gent and McWilliams 1990) beneath the mixed layer. This was already proposed by Marshall (1997). Caution should be made, however, because the agreement between eddy transport of mode water and eddy (induced) subduction of mode water in the present model only counts in the integrated sense and is associated with much more complicated circulation paths than in two-dimensional models. The agreement between eddy transport and the eddy contribution to subduction and net entrainment/detrainment in the present model could be fortuitous and should be tested in more general circumstances. Also, the absolute values of the different quantities found in this study may be influenced by the

idealized model configuration and should be tested in a more realistic context.

Acknowledgments. We thank Will de Ruijter for his valuable comments on this manuscript. Also, the reviewers are acknowledged for their comments. This research was supported by The Netherlands Organization for Scientific Research (NWO), project VVA-770-03-252. The computations have been performed on the Fujitsu VPP-700 of the ECMWF in Reading.

REFERENCES

Bleck, R., and D. B. Boudra, 1986: Wind-driven spin-up in eddy-resolving ocean models formulated in isopycnic and isobaric coordinates. *J. Geophys. Res.,* **91,** 7611–7621.

——, H. P. Hanson, D. Hu, and E. B. Kraus, 1989: Mixed layer–thermocline interaction in a three-dimensional isopycnic coordinate model. *J. Phys. Oceanogr.,* **19,** 1417–1439.

——, C. Rooth, D. Hu, and L. T. Smith, 1992: Salinity-driven thermocline transients in a wind- and thermohaline-forced isopycnic coordinate model of the North Atlantic. *J. Phys. Oceanogr.,* **22,** 1486–1505.

Böning, C. W., and R. C. Budich, 1992: Eddy dynamics in a primitive equation model: Sensitivity to horizontal resolution and friction. *J. Phys. Oceanogr.,* **22,** 361–381.

Bryan, K., 1991: Poleward heat transport in the ocean. *Tellus,* **43,** 104–115.

Cox, M. D., 1985: An eddy-resolving numerical model of the ventilated thermocline. *J. Phys. Oceanogr.,* **15,** 1312–1324.

——, 1987: An eddy-resolving numerical model of the ventilated thermocline: Time dependence. *J. Phys. Oceanogr.,* **17,** 1044–1056.

Cushman-Roisin, B., 1987: Subduction. *Dynamics of the Oceanic Surface Mixed Layer,* Hawaii Institute of Geophysics Special Publications. P. Müller and D. Henderson, Eds., 181–196.

Danabosoglu, G., and J. C. McWilliams, 1995: Sensitivity of the global ocean circulation to the parameterization of mesoscale tracer transports. *J. Climate,* **8,** 2967–2987.

de Ruijter, W. P. M., 1983: Effects of velocity shear in advective mixed-layer models. *J. Phys. Oceanogr.,* **13,** 1589–1599.

Drijfhout, S. S., 1994a: On the heat transport by mesoscale eddies in an ocean circulation model. *J. Phys. Oceanogr.,* **24,** 353–369.

——, 1994b: Sensitivity of eddy-induced heat transport to diabatic forcing. *J. Geophys. Res.,* **99,** 18 481–18 499.

——, and F. H. Walsteijn, 1998: Eddy-induced heat transport in a coupled ocean–atmospheric anomaly model. *J. Phys. Oceanogr.,* **28,** 250–266.

Follows, M. J., and J. C. Marshall, 1994: Eddy driven exchange at ocean fronts. *Ocean Modelling* (unpublished manuscripts), **102,** 5–9.

Garrett, C., and A. Tandon, 1997: The effects on water mass formation of surface mixed layer time dependence and entrainment fluxes. *Deep-Sea Res.,* **44,** 1991–2006.

——, K. Speer, and E. Tragou, 1995: The relationship between water mass formation and the surface buoyancy flux, with application to Philips' Red Sea model. *J. Phys. Oceanogr.,* **25,** 1696–1705.

Gent, P. R., and J. C. McWilliams, 1990: Isopycnal mixing in ocean circulation models. *J. Phys. Oceanogr.,* **20,** 150–155.

Hazeleger, W., and S. S. Drijfhout, 1998: Mode water variability in a model of the subtropical gyre: Response to anomalous forcing. *J. Phys. Oceanogr.,* **28,** 266–288.

——, and ——, 1999: Stochastically forced mode water variability. *J. Phys. Oceanogr.,* **29,** 1772–1786.

Jenkins, W. J., 1988: The use of anthropogenic tritium and helium-3 to study subtropical gyre ventilation and circulation. *Philos. Trans. Roy. Soc. London, Ser. A,* **325,** 43–61.

Luksch, U., and, H. von Storch, 1992: Modeling the low-frequency sea surface temperature variability in the North Pacific. *J. Climate,* **5,** 893–906.

Marsh, R., and A. L. New, 1996: Modeling 18° water variability. *J. Phys. Oceanogr.,* **26,** 1059–1080.

Marshall, D., 1997: Subduction of water masses in an eddying ocean. *J. Mar. Res.,* **55,** 201–222.

——, and J. C. Marshall, 1995: On the thermodynamics of subduction. *J. Phys. Oceanogr.,* **25,** 138–151.

Marshall, J. C., A. J. G Nurser, and R. G. Williams, 1993: Inferring the subduction rate and period over the North Atlantic. *J. Phys. Oceanogr.,* **23,** 1315–1329.

——, D. Jamous, and J. Nilsson, 1998: Reconciling ''thermodynamic'' and ''dynamic'' methods of computation of water mass transformation rates. *Deep-Sea Res.,* **46,** 545–572.

McGillicuddy, D. J., Jr., and Coauthors, 1998: Influence of mesoscale eddies on new production in the Sargasso Sea. *Nature,* **394,** 263–266.

Oschlies, A., and V. Garcon, 1998: Eddy-induced enhancement of primary production in a model of the North Atlantic Ocean. *Nature,* **394,** 266–269.

Pierce, S. P., and T. J. Joyce, 1988: Gulf Stream velocity and structure through inversion of hydrographic and acoustic Doppler data. *J. Geophys. Res.,* **93,** 2227–2236.

Qiu, B., and R. X. Huang, 1995: Ventilation of the North Atlantic and North Pacific: Subduction versus obduction. *J. Phys. Oceanogr.,* **25,** 2374–2390.

Spall, M. A., 1995: Frontogenesis, subduction and cross-front exchange at upper-ocean fronts. *J. Geophys. Res.,* **100,** 2543–2557.

Speer, K., and E. Tziperman, 1992: Rates of water mass formation in the North Atlantic Ocean. *J. Phys. Oceanogr.,* **22,** 93–104.

Stull, R. B., 1988: *An Introduction to Boundary Layer Meteorology.* Kluwer Academic, 666 pp.

Sutton, R. T., and M. R. Allen, 1997: Decadal predictability of North Atlantic sea surface temperature and climate. *Nature,* **388,** 563–567.

Tziperman, E., 1986: On the role of interior mixing and air–sea fluxes in determining the stratification and circulation of the oceans. *J. Phys. Oceanogr.,* **16,** 680–693.

Walin, G., 1982: On the relation between sea-surface heat flow and thermal circulation in the ocean. *Tellus,* **34,** 187–195.

Woods, J. D., 1985: The physics of thermocline ventilation. *Coupled Ocean–Atmosphere Models,* J. C. J. Nihoul, Ed., Elsevier, 543–590.

——, and W. Barkmann, 1986: A lagrangian mixed layer model of Atlantic 18°C water formation. *Nature,* **319,** 574–576.

Worthington, L. V., 1959: The 18° water in the Sargasso Sea. *Deep-Sea Res.,* **5,** 297–305.

Zhang, R., and S. Levitus, 1997: Structure and cycle of decadal variability of upper ocean temperature in the North Pacific. *J. Climate,* **10,** 710–727.

Zorita, E., and C. Frankignoul, 1997: Modes of North Atlantic decadal variability in the ECHAM1/LSG coupled ocean–atmosphere general circulation model. *J. Climate,* **10,** 183–200.